JPEDAV (2006) 27:353-362
DOI: 10.1361/154770306X116289
1547-7037/$19.00 ©ASM International

Thermodynamic Reassessment of the Cr-O System in the Framework of Solid Oxide Fuel Cell (SOFC) Research

Erwin Povoden, A. Nicholas Grundy, and Ludwig J. Gauckler

(Submitted August 10, 2005; in revised form March 1, 2006)

A comprehensive compilation and evaluation of experimental and thermodynamic data for the Cr-O system is presented and, by application of the CALPHAD method, a consistent set of thermodynamic model parameters is optimized based on new experiments. Nonstoichiometry of eskolaite ($Cr_2O_{3-\delta}$) is described using the compound energy model, and the liquid is described using the two-sublattice model for ionic liquids. Cr_3O_4 is described as a stoichiometric compound. Also the magnetic transition in Cr_2O_3 and the oxygen solubility in Cr are modeled.

Keywords aging, assessment, binary, CALPHAD, optimization, phase diagram, thermodynamic modeling

1. Introduction

Solid oxide fuel cells (SOFC) offer high fuel conversion efficiencies and, due to their high operating temperature (>1173 K), combined heat and power-generation capability. For the planar design SOFC, which offers low fabrication costs, ceramic and metal interconnect materials have been tested and evaluated over the years. Meanwhile, the use of Cr-base alloy interconnect materials has gained popularity due to their relative ease of fabrication, low machining costs, and high thermal conductivity.[1] Namely a Cr5Fe1Y_2O_3 oxide dispersion strengthened alloy with the composition 94% Cr, 5% Fe, and 1% Y_2O_3 developed jointly by Plansee and Siemens with excellent material properties has been promoted as a suitable alternative to the earth alkaline doped $LaCrO_3$ ceramics interconnect. However, the use of this alloy as an interconnect material in SOFCs leads to the degradation of the fuel cell performance especially on the cathode side of the fuel cell. Loss of performance caused by the migration of Cr originating from the alloy interconnect is well documented by several investigators. Microstructural analyses of the cathode of SOFC cells show the formation of Cr_2O_3 and $(Mn, Cr)_3O_4$, which block active sites as well as pores, thus substantially reducing the triple-phase boundary area for the normal oxygen reduction reaction at the cathode/electrolyte interface.

The influence of Cr from the interconnect alloy on the strontium-doped lanthanum manganite (LSM) cathode can be modeled in terms of an equilibrium thermodynamic view to contribute to strategies for reducing the SOFC chromium poisoning process by optimizing SOFC operating conditions and refining SOFC material compositions.

Erwin Povoden and **Ludwig J. Gauckler,** Institute of Nonmetallic Materials, Dept. of Materials, Swiss Federal Institute of Technology (ETH-Zurich) Hönggerberg, Wolfgang-Pauli-Strasse 10, HCI G 530, CH-8092 Zürich, Switzerland; and **A. Nicholas Grundy,** Centre of Research in Computational Thermochemistry (CRCT), École Polytechnique, P.O. Box 6079, Station "Downtown," Montréal, Québec, Canada H3C7. Contact e-mail: erwin.povoden@mat.ethz.ch.

2. Experimental Data

2.1 Phase Diagram Data

Experimental investigations of phase diagrams in the Cr-O system were made by Ol'shanskii and Shlepov[2] and Toker.[3] These authors document the existence of a large miscibility gap between the metallic and the oxide melt. Eskolaite (Cr_2O_3) is the dominating stable oxide phase over a wide temperature range. Results of special points in the Cr-O phase diagram from several studies are summarized in Table 1. The melting temperatures of eskolaite in air reported from Kanolt[4] and Wilde and Rees[5] can be discarded as being too low. McNally[6] measured a melting temperature of 2603 K in air using an induction furnace. This value significantly deviates from the result of Bunting,[7] who measured 2543 ± 25 K also in air. Grube and Knabe[8] found that 1 wt.% Cr_2O_3 lowers the melting point of metallic Cr from 2163 K to between 2043 and 2063 K. Lam[9] reported the existence of molten chromium with oxygen impurities of 1400 ppm at 2133 K. The monotectic reaction of Cr (bcc) metal and liquid was found at 2083 K by Grube and Knabe[8] and by Ol'shanskii and Shlepov.[2] The question of the existence of a crystalline Cr_3O_4 phase was discussed controversially by several authors. Investigations made by Hilty et al.[10] and Hook and Adair[11] led them to postulate the existence of a crystalline Cr_3O_4 phase in the Cr-Fe-O system. Concerning the pure Cr-O system, Ol'shanskii and Shlepov[2] and Johnson and Muan[12] did not find Cr_3O_4 up to the eutectic temperature of chromium oxide, whereas Toker et al.[13] concluded from microstructural observations and a discontinuity in the slopes of the temperature-oxygen pressure curves for univariant equilibria involving metallic Cr and various chromium oxide phases that a Cr_3O_4 phase exists in a narrow temperature range between 1923 and 1978 K. Microstructures of a

Table 1 Special points in the Cr–O system

Melting T of Cr_2O_3 in air, K	Eutectic T, K	Eutectic composition, x(O)	Cr_3O_4 detected	Stability T range of Cr_3O_4, K	Monotectic T, K	Ref
2257	…	…	…	…	…	Kanolt[4] experimental
2317	…	…	…	…	…	Wilde and Rees[5] experimental
2603	…	…	…	…	…	McNally et al.[6] experimental
2543 ± 15	…	…	…	…	…	Bunting[7] experimental
…	1933	0.52	No	…	2083	Oh'shanskii and Shlepov[2] experimental
…	1918	0.523	No	…	2083	Johnson and Muan[12] experimental
2571	1941	0.513	Yes	1923 to 1978	…	Degterov and Pelton[39] calculated
…	1929	0.496	Yes	1918 to 1974	2160	Kowalski and Spencer[40] calculated
…	1937	0.499	Yes	1923 to 1978	2130	Talor and Dinsdale[41] calculated
…	*1938 ± 2*	*0.497*	Yes	*1923 ± 2* to *1978 ± 3*	2083	Toker et al.[13] experimental
2539	1938	0.497	Yes	1918 to 1973	2117	This work, calculated

Note: Italicized data were used for optimization.

quenched chromium melt with maximum oxygen impurities of about 2930 ppm lately investigated by Lam[9] document an inner Cr_3O_4 phase and an outer Cr_2O_3 phase in dispersed oxides in large chromium grains and grain boundaries. This indicates that the first phase to crystallize on solidification is Cr_3O_4, giving strong evidence for the stability of this phase. Thus in this study the authors accept the findings of Toker et al.[13] and Lam.[9]

2.2 Thermodynamic Data

2.2.1 Oxygen Potentials. Grube and Flad[14] measured log (P_{O_2}) values for the Cr-Cr_2O_3 equilibrium between 1053 and 1573 K by both oxidizing Cr to Cr_2O_3 and reducing Cr_2O_3 to Cr in a flowing H_2-H_2O atmosphere. At temperatures $\geq$1573 K they were confronted with the loss of a quarter of Cr in the case of oxidation; thus at these temperatures log (P_{O_2}) values were determined solely from the reduction of Cr_2O_3. Novokhatskii and Lenev[15] studied the equilibrium of the reduction of Cr_2O_3 to Cr with hydrogen from 1493 to 1893 K. These authors used a flow method where thermal diffusion problems were suppressed by inserting corundum bushes into the reaction tube. Appreciable sublimation of metallic chromium was not observed. Davies and Smeltzer[16] determined log (P_{O_2}) values of Cr_2O_3 at 1173, 1273, and 1373 K, using an electrochemical cell with a calcia-zirconia electrolyte and a Fe/FeO reference electrode. Toker et al.[13] measured log (P_{O_2}) values of Cr_2O_3 by equilibrating Cr and Cr_2O_3 in H_2-CO_2 mixtures of known oxygen potentials at temperatures from 1773 to 2098 K. Pehlke et al.[17] used two separate series of emf measurements employing the solid oxide electrolyte galvanic cell technique from 1148 to 1548 K. The reversibility and accuracy of the yttria-doped thoria electrolyte and the electrode was tested by measurements of a standard iron-chromium alloy at 1326 K. The independent results of corrected cell potentials of the two measurement series are excellent. The data are in close agreement with the gas-solid equilibrium measurements by Jeannin et al.[18] Disagreement between the emf results from Pehlke et al.,[17] Pugliese and Fitterer,[19] and Tretjakow and Schmalzried[20] were assigned to possible electronic conduction in the zirconia electrolyte used by the latter authors, as well as transport of oxygen ions from the cathode to the Cr/Cr_2O_3 anode. Applying the same technique as Pehlke et al.,[17] Holzheid and O'Neill[21] noted a deviation from the well-established trend at 900 to 1300 K for high-temperature data caused by finite electronic conductivity at elevated temperatures, causing transfer of oxygen through the cell, as well as the importance of sufficient time to attain equilibrium, that is, days for $T < 1100$ K. The obtained dissociation pressures of Cr_2O_3 are in agreement with average values derived from emf studies using an yttria-doped thoria electrolyte worked out by Jacob[22] and a very high-temperature gas-mixing study of Toker et al.[13]

2.2.2 Heat Capacities, Heat Contents, and Entropies. Anderson's[23] calorimetric data set of C_p-values lacks detailed documentation of the experimental procedure. Bruce and Cannell[24] applied a two-dimensional temperature wave method using a single crystal of Cr_2O_3 to calculate specific heat in the temperature range $290.68 \leq T \leq 323.43$ K, and fitted the data to the heat of diffusion equation employing a least-mean-squares fit to the heat of diffusion equation that considers some material properties. The accuracy of this study is evident from excellent data reproduction by performing two runs in the entire temperature range. Documentation of the experiments, data presentation, and fitting procedure were worked out very carefully. Resulting C_p data correspond nicely to the most recent calorimetric results from Klemme et al.[25] The latter authors measured a consistent data set of heat capacities of synthetic eskolaite from 1.5 to 340 K with mean increments of 0.56 K. Uncertainties of 0.4% for C_p (20 K < T < 200 K) and 0.7% for C_p (T < 20 K) were estimated. For C_p° (Cr_2O_3) = 120.37 J/K · mol, Chase et al.[26] relied on the calculated results from heat content measurements performed by Kelley et al.[27] The latter authors fitted their data measured from 400 to 1800 K by:

$$H_T^\circ - H_{298.16}^\circ = aT + \frac{b}{2}T^2 + cT^{-1} + d \quad \text{(Eq 1)}$$

yielding

$$H^{\circ}_{T} - H^{\circ}_{298.16} = 28.53T + 1.10 \times 10^{-3}\, T^2 + 3.736 \times 10^{5}\, T^{-1} - 9759 \quad \text{(Eq 2)}$$

Temperature derivation of Eq 2 results in:

$$C_p = 28.53 + 2.20 \times 10^{-3}\, T - 3.736 \times 10^{5}\, T^{-2} \quad \text{(Eq 3)}$$

For S°_{298} Cr_2O_3) Chase et al.[26] relied on the results from Anderson,[23] who calculated S°_{298} (Cr_2O_3) = 81.17 ± 0.84 J/K · mol by a graphical method of plotting the heat capacity against the logarithm of the temperature and modeling the heat capacity curves with Debye functions. This procedure was critically documented by other authors, for example, Klemme et al.[25] Klemme et al.[25] recommend S°_{298} (Cr_2O_3) = 83.1 J/K · mol by reevaluating emf data from Holzheid and O'Neill,[21] who calculated S°_{298} (Cr_2O_3) = 85.74 ± 1.3 J/K · mol from their measurements. Dellien et al.[28] adopted their S°_{298} (Cr_2O_3) value from Wagman et al.[29]

Shirokov[30] estimated S°_{298} of a highly metastable CrO phase to be 46.86 J/K · mol.

2.2.3 Enthalpies of Formation. Roth and Wolf[31] found $\Delta_f H^{\circ}_{298}$ (Cr_2O_3) = −1125.8 ± 2.5 kJ/mol by applying a calorimetric technique. Mah,[32] using a bomb calorimetric combustion technique at 1323 K and 30 atm oxygen pressure, calculated $\Delta_f H^{\circ}_{298}$ (Cr_2O_3) = −1140.98 ± 1.7 kJ/mol. Some difficulty caused by moisture adsorption was encountered in weighing the combustion products. This was circumvented by heating the combustion products to 1323 K. For the calculation of $\Delta_f H^{\circ}_{298}$ (Cr_2O_3) the heat content data given by Kelley et al.[27] were used. Ramsey et al.[33] used heat capacity and entropy data from tabulations of Coughlin[34] to obtain $\Delta_f H^{\circ}_{298}$ (Cr_2O_3) = −1122.06 kJ/mol. Navrotsky[35] cited Garrels and Christ[36] for $\Delta_f H^{\circ}_{298}$ (Cr_2O_3) = −1128.42 kJ/mol. Chase et al.[26] evaluated $\Delta_f H^{\circ}_{298}$ (Cr_2O_3) = −1134.7 ± 8.4 kJ/mol from several earlier studies, while Dellien et al.[28] adopted $\Delta_f H^{\circ}_{298}$ (Cr_2O_3) = −1139.72 kJ/mol from Wagman et al.[29] Klemme et al.[25] recommend $\Delta_f H^{\circ}_{298}$ (Cr_2O_3) = −1128.2 ± 0.4 kJ/mol by evaluating emf data from Holzheid and O'Neill.[21]

Shirokov[30] estimated $\Delta_f H^{\circ}_{298}$ (CrO) = −305.4 kJ/mol for metastable CrO.

3. Previous Assessments of the Cr-O System

Banik et al.[37] established a phase diagram for the Cr-O system based on a subregular solution model that is in good agreement with experimental data obtained by Ol'shanskii and Shlepov,[2] thermodynamic data for Cr-Cr_2O_3 from Fromm and Gebhardt,[38] and thermodynamic estimates for CrO from Shirokov.[30] Degterov and Pelton[39] reassessed the CrO-Cr_2O_3 subsystem, using a modified quasi-chemical model for the molten slag database. Their calculated liquidus temperature of Cr_2O_3 in air is 2571.16 K, which is in good agreement with an early finding by Bunting[7] who measured 2543 ± 25 K. Kowalski and Spencer[40] used the associated solution model for the liquid phase based on the experimental data used by Taylor and Dinsdale.[41] The latter authors proposed a phase diagram in good agreement with the experimental data obtained by Toker,[3] using the same thermodynamic models as the authors use in this work, which are the two-sublattice ionic model for the liquid and the compound energy model for the Cr_2O_3 phase. Taylor and Dinsdale[41] fitted C_p data from Anderson[23] close to the antiferromagnetic to paramagnetic transition and data from Chase et al.[26] at elevated temperatures as a sum of magnetic and nonmagnetic contributions. Experimental information on phase relations for their assessment were taken from Ol'shanskii and Shlepov,[2] Toker,[3] Kelley et al.,[27] and Grube and Knabe.[8] The heat capacity of Cr_3O_4 was taken as 7/5 times the nonmagnetic value for Cr_2O_3 according to Neumann and Kopp's rule. Their calculated values for the enthalpy of formation and the entropy of Cr_3O_4 are in agreement with an estimate done by Chipman.[42]

Their optimization of one of the charged endpoints in their compound energy model for eskolaite and the use of six interaction parameters to describe the liquid may lead to problems on extrapolation to higher-order systems, especially as their miscibility gap does not close on increasing temperature. The use of six parameters for the description of the Cr_3O_4 phase is somewhat incommensurate with the scanty experimental information of this phase.

There is a large uncertainty concerning the exact melting point of Cr_2O_3, and only few thermodynamic data of the Cr_3O_4 phase and the liquid phase exist. This is reflected by significant variations of the position of the eutectics, the stability field of Cr_3O_4, and the temperature of the monotectic reaction of Cr (bcc) and liquid between the assessments of the Cr-O system.

4. Thermodynamic Modeling

4.1 Solid Phases

The crystal structure of eskolaite is α-Al_2O_3 type, space group $R\bar{3}c$. Eskolaite shows an antiferromagnetic to paramagnetic transition at 305.5 K. The magnetic properties of eskolaite can be described using a magnetic ordering model proposed by Inden,[43] and simplified by Hillert and Jarl.[44] In this model, a magnetic contribution to the Gibbs energy is added to the nonmagnetic part of the Gibbs energy given as:

$$\Delta G^{MAG}_{m} = RT\ln(\beta + 1) f(\tau) \quad \text{(Eq 4)}$$

where β is a parameter related to the total magnetic entropy, and $\tau = T/T_c$. T_c is the critical temperature for magnetic ordering. T_c and β are both dependent on the composition. The magnetic parameter p equals 0.28.

The oxygen nonstoichiometry of Cr_2O_3 with the sublattice occupation $(Cr^{2+},Cr^{3+})_2$ $(Cr^{3+},Va)_1$ $(O^{2-})_3$ can be modeled using experimental data from Matsui and Naito.[45] This means that reduction is accomplished by the formation of interstitial Cr^{3+} and not by the formation of oxygen vacancies, which is in agreement with Young et al.[46] When modeling oxygen deficiency in an oxide phase, it is impor-

tant to submit the experimental data to a defect-chemistry analysis. In the case of $Cr_2O_{3-\delta}$ modeled with interstitial Cr^{3+} the defect reaction reads:

$$2Cr_{Cr}^{x} + Va_i^{x} + 3O_O^{x} \rightarrow \tfrac{3}{2}Cr'_{Cr} + \tfrac{1}{2}Cr_i^{\cdot\cdot\cdot} + \tfrac{1}{4}Va_i^{x} + \tfrac{9}{4}O_O^{x} + \tfrac{3}{8}O_2\,(g) \quad \text{(Eq 5)}$$

giving the equilibrium constant

$$K_r = \frac{[Cr'_{Cr}]^{3/2}[Cr_i^{\cdot\cdot\cdot}]^{1/2}[Va_i^{x}]^{1/4}[O_O^{x}]^{9/4}P_{O_2}^{3/8}}{[Cr_{Cr}^{x}]^2[Va_i^{x}][O_O^{x}]^3} \quad \text{(Eq 6)}$$

Assuming small defect concentrations all concentrations except $[Cr'_{Cr}]$ and $[Cr_i^{\cdot\cdot\cdot}]$ are ~1 and can be ignored. Due to charge neutrality, the relation $[Cr_i^{\cdot\cdot\cdot}] = 3[Cr'_{Cr}]$ must hold. Inserting this into Eq 6 gives the proportionalities $[Cr_i^{\cdot\cdot\cdot}] \propto P_{O_2}^{-3/16}$ and $[Cr'_{Cr}] \propto P_{O_2}^{-3/16}$. To explain their experimental results Matsui and Naito[45] proposed a defect reaction that leads to the same proportionality; however, their equation violates the fundamentals of defect chemistry and must be rejected in favor of the defect reaction given above (Eq 5 and 6). The following other interstitial defects could be assumed: $Cr_i^{\cdot\cdot\cdot}$ giving a slope of $P_{O_2}^{-1/4}$, and $Cr_i^{\cdot\cdot\cdot}$ giving a slope of $P_{O_2}^{-3/20}$. Both are unlikely, the former because it is unlikely to get Cr^{4+} on reduction, the latter because of the large size of Cr^{2+}. Assuming the defect reaction:

$$Cr_{Cr}^{x} + \tfrac{1}{2}O_O^{x} \rightarrow Cr'_{Cr} + \tfrac{1}{2}Va_O^{\cdot\cdot} + \tfrac{1}{4}O_2\,(g) \quad \text{(Eq 7)}$$

leads to a proportionality of $[Va_O^{\cdot\cdot}] \propto P_{O_2}^{-1/6}$ and $[Cr'_{Cr}] \propto P_{O_2}^{-1/6}$. This slope does not correspond to the experimental findings of Matsui and Naito.[45] Also the defects cannot explain the electrical properties measured by Young et al.[46]

The low nonstoichiometry data from Matsui and Naito[45] show a different slope than their higher nonstoichiometry data. In contrast to Matsui and Naito[45] who explain this assuming that neutral Cr forms interstitially, the present authors believe that the different slopes are caused by a competing defect reaction, for example charge disproportionation, $2Cr^{3+} \rightarrow Cr^{2+} + Cr^{4+}$, similar to the case of $LaMnO_3$ perovskites.[47] The present authors did not consider this by their defect chemistry model, as it would make the description quite complex.

Figure 1 is a graphic representation of the model the authors use to describe the oxygen nonstoichiometry of eskolaite, where each corner of the composition square represents a °*G* parameter. The four corner compositions represent all possibilities to express the Cr_2O_3 phase according to the above formula for the sublattice occupation. The corner Cr^{3+}:Va:O^{2-} corresponds to stoichiometric Cr_2O_3. The three other corner compositions present charged compounds. Only compounds along the neutral line can exist on their own. As the most reasonable way to model reduction is to use the reduced neutral endpoint $(Cr^{2+})_2\,(Cr^{3+}_{2/3}Va_{1/3})_1\,(O^{2-})_3$, labeled A in Fig. 1, one has to find functions of °*G* of three charged corners expressed solely in terms of the neutral compositions. This is done by using the two equations for the stoichiometric and the reduced endpoints, by choosing an arbitrary reference, and by defining a reciprocal reaction giving four equations with which all °*G*s at the corners can be expressed.

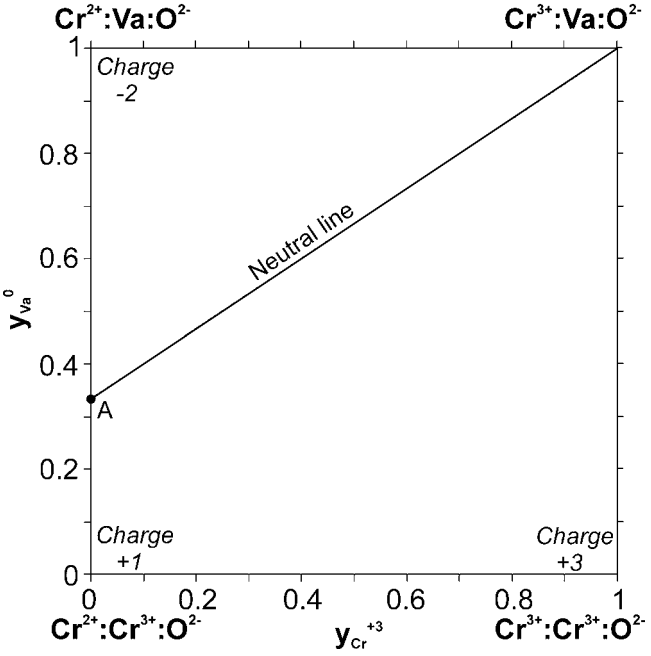

Fig. 1 Compound energy model for the $Cr_2O_{3-\delta}$ phase

The function to model the reduction then reads:

$$^{\circ}G_{Cr_2^{2+}(Cr_{2/3}^{3+}Va_{1/3})(O^{2-})_3} = {}^{\circ}G_{Cr_2O_3} + \tfrac{2}{3}{}^{\circ}G_{Cr}^{SER} + A + BT + RT(\tfrac{2}{3}\ln\tfrac{2}{3} + \tfrac{1}{3}\ln\tfrac{1}{3}) \quad \text{(Eq 8)}$$

The last term describes the configurational entropy due to mixing of Cr^{3+} and Va on the interstitial site. °*G* of the 3+ charged end member $(Cr^{3+})_2\,(Cr^{3+})_1\,(O^{2-})_3$ is chosen as reference and given the value $^{\circ}G_{Cr^{3+}:Cr^{3+}}$. Then the reciprocal relation reads

$$^{\circ}G_{Cr^{3+}:Cr^{3+}} + {}^{\circ}G_{Cr^{2+}:Va} = {}^{\circ}G_{Cr^{3+}:Va} + {}^{\circ}G_{Cr^{2+}:Cr^{3+}} = \Delta G_r \quad \text{(Eq 9)}$$

To avoid the inevitable formation of miscibility gaps if the energy of the reciprocal relation is large we set this energy zero, which leads to:

$$^{\circ}G_{Cr^{3+}:Cr^{3+}} + {}^{\circ}G_{Cr^{2+}:Va} - {}^{\circ}G_{Cr^{3+}:Va} - G_{Cr^{2+}:Cr^{3+}} = 0 \quad \text{(Eq 10)}$$

This means that without introducing interaction parameters one gets an ideal description between Cr_2O_3 and $Cr_2O_{3-\delta}$. The expressions for all °*G*s at the corners resulting from Eq 8 to 10 are listed in Table 2.

In contrast to Taylor and Dinsdale,[41] who needed four parameters to model the Cr_2O_3 phase and had to arbitrarily equate the °*G* of $(Cr^{2+})_2\,(Va)_1\,(O^{2-})_3$ to stoichiometric Cr_2O_3, the latter constraint is not needed in this model, and one can reduce the number of parameters to only two.

The oxygen solubility in solid Cr (bcc) can be described by an interstitial solution model of the form $(Cr)_1(O,Va)_3$. For this model, literature data from Caplan et al.[48] are used. It was not possible to model the oxygen solubility using the end member $^{\circ}G_{Cr:O}$ as this end member turned

Table 2 Thermodynamic description of the Cr–O system

Element	Element reference	Mass	H_{298}-H_0	S_{298}
Cr	Cr-bcc-A2	51.996	4050.0	23.543
O	½ mol O_2	15.999	4341.0	102.52

Liquid

$(Cr^{2+},Cr^{3+})_p(O^{2-},Va^{q-})_q$

$p = 2y_{O^{2-}} + qy_{Va}$, $q = 2y_{Cr^{2+}} + 3y_{Cr^{3+}}$

${}^{\circ}G^{L}_{Cr^{2+}:Va^{q-}} - H^{SER}_{Cr} = GCR\_L$

${}^{\circ}G^{L}_{Cr^{3+}:Va^{q-}} - H^{SER}_{Cr} = 2GCR\_L + GCR2O3\_L - 3GCR1O1\_L$

${}^{\circ}G^{L}_{Cr^{3+}:O^{2-}} - 2H^{SER}_{Cr} - 3H^{SER}_{O} = GCR2O3\_L$

${}^{\circ}G^{L}_{Cr^{2+}:O^{2-}} - 2H^{SER}_{Cr} - 2H^{SER}_{O} = 2GCR1O1\_L$

${}^{\circ}L_{Cr^{2+}:O^{2-},Va^{q-}} = {}^{\circ}L_{Cr^{3+}:O^{2-},Va^{q-}} = 121{,}000$

Solid Cr (bcc_A2)

$(Cr)_1(O, Va)_3$

${}^{\circ}G^{bcc}_{Cr:Va} - H^{SER}_{Cr} = GHSERCR$

${}^{\circ}G^{bcc}_{Cr:O} - H^{SER}_{Cr} - 3H^{SER}_{O} = GHSERCR + 3\ GHSEROO + 243T$

$L^{bcc}_{Cr:O,Va} = -709{,}542$

$p = 0.4$; $T_c = -311.5$; $\beta = -0.008$

Solid Cr (cph_A3)

${}^{\circ}G^{cph}_{CrVa} - H^{SER}_{Cr} = GCRHCP$

$p = 0.28$; $T_c = -1109$; $\beta = -2.46$

Solid Cr (fcc_A1)

${}^{\circ}G^{fcc}_{Cr:Va} - H^{SER}_{Cr} = GCRFCC$

$p = 0.28$; $T_c = -1109$; $\beta = -2.46$

Solid Cr (bcc_A12)

${}^{\circ}G^{bcca12}_{Cr:Va} - H^{SER}_{Cr} = GCRBCCA12$

Solid Cr (cub_A13)

${}^{\circ}G^{cub}_{Cr:Va} - H^{SER}_{Cr} = GCRCUB$

CrO

${}^{\circ}G^{Cr_1O_1}_{Cr:O} - H^{SER}_{Cr} - H^{SER}_{O} = GCR1O1$

Cr_2O_3

$(Cr^{2+},Cr^{3+})_2\ (Cr^{3+}, Va)_1\ (O^{2-})_3$

${}^{\circ}G^{Cr_2O_3}_{Cr^{3+}:Va:O^{2-}} - 2H^{SER}_{Cr} - 3H^{SER}_{O} = GCR2O3$

${}^{\circ}G^{Cr_2O_3}_{Cr^{3+}:Cr^{3+}:O^{2-}} - 3H^{SER}_{Cr} - 3H^{SER}_{O} = GCR2O3 + GHSERCR$

${}^{\circ}G^{Cr_2O_3}_{Cr^{2+}:Cr^{3+}:O^{2-}} - 3H^{SER}_{Cr} - 3H^{SER}_{O} = GCRO0 + \tfrac{1}{3}GHSERCR - 5.2923T$

${}^{\circ}G^{Cr_2O_3}_{Cr^{2+}:Va:O^{2-}} - 3H^{SER}_{Cr} - 3H^{SER}_{O} = GCRO0 - \tfrac{2}{3}GHSERCR - 5.2923T$

$p = 0.28$; $T_c = 308.6$; $\beta = 3.0$

Cr_3O_4

${}^{\circ}G^{Cr_3O_4}_{Cr:O} - 3H^{SER}_{Cr} - 4H^{SER}_{O} = GCR3O4$

Element	Element reference	Mass	H_{298}-H_0	S_{298}

Functions

GHSERCR = $298.15 < T < 2180$

$-8856.94 + 157.48T - 26.908T \ln T + 0.00189435T^2$

$-1.47721 \times 10^{-6}\ T^3 + 139{,}250T^{-1}$

$2180 < T < 6000$

$-34{,}869.344 + 344.18T - 50.0T \ln T - 2.88526 \times 10^{32}\ T^{-9}$

GCRHCP = $298.15 < T < 2180$

$-4{,}418.94 + 157.48T - 26.908T \ln T + 0.00189435T^2$

$-1.47721 \times 10^{-6}\ T^3 + 139{,}250T^{-1}$

$2180 < T < 6000$

$-30{,}431.344 + 344.18T - 50.0T \ln T - 2.88526 \times 10^{32}\ T^{-9}$

GCRFCC = $298.15 < T < 2180$

$-1572.94 + 157.643T - 26.908T \ln T + 0.00189435T^2$

$-1.47721 \times 10^{-6}\ T^3 + 139{,}250T^{-1}$

$2180 < T < 6000$

$-27{,}585.344 + 344.343T - 50T \ln T - 2.88526 \times 10^{32}\ T^{-9}$

GCRBCCA12 = $298.15 < T < 2180$

$2230.06 + 160.1996T - 26.908T \ln T + 0.00189435T^2$

$-1.47721 \times 10^{-6}\ T^3 + 139{,}250T^{-1}$

$2180 < T < 6000$

$-23{,}782.344 + 346.8996T - 50T \ln T - 2.88526 \times 10^{32}\ T^{-9}$

GCRCUB = $298.15 < T < 2180$

$7042.06 + 158.1076T - 26.908T \ln T + 0.00189435T^2$

$-1.47721 \times 10^{-6}\ T^3 + 139{,}250T^{-1}$

$2180 < T < 6000$

$-18{,}970.344 + 344.8076T - 50\ T \ln T - 2.88526 \times 10^{32}\ T^{-9}$

GHSEROO = $298 < T < 1000$

$-3480.872255 - 25.5028601T - 11.1355068T \ln T - 0.005098873T^2$
$+ 6.6184604 \times 10^{-7}\ T^3 - 38{,}364.8742T^{-1}$

$1000 < T < 3000$

$-6568.76015 + 12.66000166T - 16.8138015T \ln T - 5.9579637 \times 10^{-4}\ T^2$
$+ 6.78055555 \times 10^{-9}\ T^3 + 262{,}904.778T^{-1}$

$3300 < T < 6000$

$-13{,}986.728 + 31.259625T - 18.9536T \ln T - 4.25243 \times 10^{-4}\ T^2$
$+ 1.0721 \times 10^{-8}\ T^3 + 4{,}383{,}200T^{-1}$

GCR2O3 = $-1{,}164{,}542 + 728.56T - 119.8T \ln T$
$-4.97 \times 10^{-3}\ T^2 + 1{,}050{,}000\,T^{-1}$

GCR1O1 = $0.5GCR2O3 - 0.5GHSEROO + 255{,}269 - 53.82T$

GCR3O4 = $1.5GCR2O3 - 0.5GHSEROO + 280{,}045 - 93.76T$

GCRO0 = $108{,}305 + GCR2O3 + \tfrac{2}{3}GHSERCR$

GCR_L = $298 < T < 2180$

$15{,}483.015 + 146.059775T - 26.908T \ln T + 0.00189435T^2$

$-1.47721 \times 10^{-6}\ T^3 + 139{,}250T^{-1} + 2.37615 \times 10^{-21}\ T^7$

$2180 < T < 6000$

$-16{,}459.984 + 335.616317T - 50T \ln T$

GCR2O3_L = $GCR2O3 + 439{,}078 - 169T$

GCR1O1_L = $0.5GCR2O3 - 0.5GHSEROO + 339{,}673 - 121.4T$

Note: All parameters are in SI units: J, mol, K, Pa: $R = 8.31451$ J/mol · K. Parameters for solid Cr, liquid Cr, and gaseous O are from Dinsdale.[49]

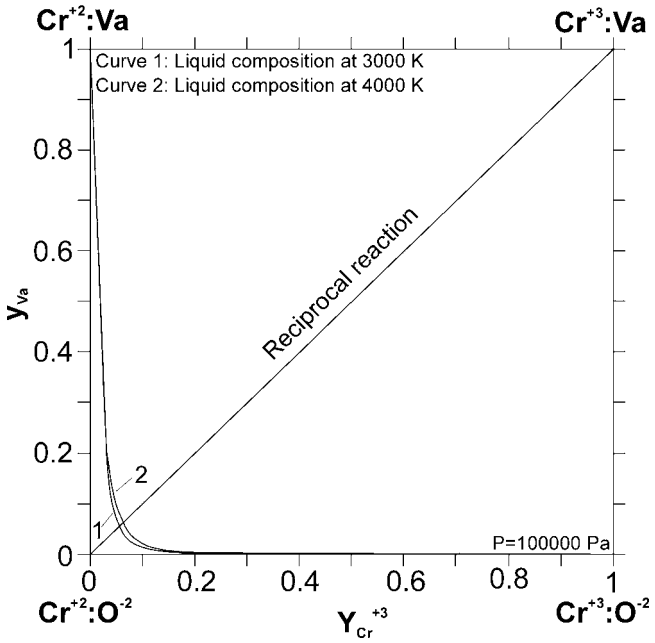

Fig. 2 Two-sublattice ionic liquid model for the Cr-O system

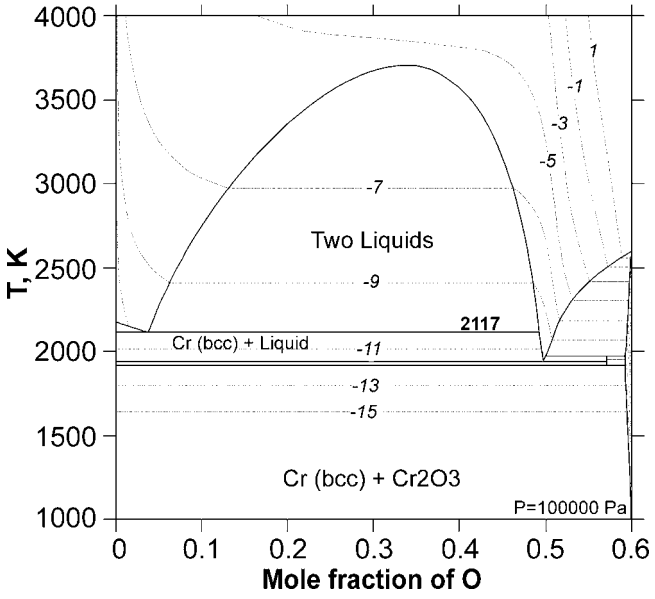

Fig. 3 Calculated Cr-O phase diagram with oxygen isobars. The gas phase was not included in the calculation.

out to be too stable and CrO_3 appeared in the stability diagram at high oxygen partial pressures. Therefore a large value is given to the end member $^{\circ}G_{Cr:O}$ (in this case 0 was a large number) and the oxygen stability is modeled with the temperature dependence of $^{\circ}G_{Cr:O}$ and a regular interaction parameter $^{\circ}L_{Cr:O,Va}$ that must of course be negative.

The Cr_3O_4 phase is based on the eskolaite phase. Its heat capacity is given by Neumann and Kopp's rule. Metastable CrO is described in the same way.

The descriptions for solid and liquid chromium metal and gaseous O_2 are from Dinsdale.[49]

4.2 Ionic Liquid

The two-sublattice ionic liquid model[50,51] is selected to describe the ionic liquid. As the experimental data on the liquid phase are scarce, the number of parameters are kept as low as possible. The sublattice occupation $(Cr^{3+},Cr^{2+})_p(O^{2-},Va^{q-})_q$ is chosen With this expression one is able to obtain reasonable results for the liquid phase using the positive interaction parameters, $^{\circ}L_{Cr^{2+}:O^{2-},Va}$, and $^{\circ}L_{Cr^{3+}:O^{2-},Va}$ that are required to give the miscibility gap. Figure 2 is a graphic expression of the model, where each corner of the composition square represents a °G parameter of the liquid phase. The four corner compositions represent all possibilities to express the liquid phase according to the above formula. The liquid composition changes along the hyperbolic curves in Fig. 2.

A special feature of the Cr-O system is the occurrence of a eutectic very close to the composition of CrO. The eutectic temperature is mainly determined by the value of the corner $Cr^{2+}:O^{2-}$.

One derives the $^{\circ}G^{L}$ functions of the oxide compositions $(Cr^{3+}:O^{2-})$ and $(Cr^{2+}:O^{2-})$ from the eskolaite phase. The $^{\circ}G^{L}$ of liquid Cr is taken from Dinsdale.[49] In this model description of the liquid phase metallic Cr-liquid can be described by both the corners Cr^{2+}:Va and Cr^{3+}:Va. Cr^{3+}:Va must be metastable compared with Cr^{2+}:Va. One way of doing this would be to simply say that Cr^{3+}:Va equals Cr^{2+}:Va plus a large positive term, for example +600,000 as given to $^{\circ}G_{Cu^{2+}:Va}$ by Hallstedt et al.[52] in his original assessment of the Cu-O system. This is however problematic for reciprocal systems. If the reciprocal energy of the system is large, there will be a tendency to form miscibility gaps as pointed out by Hillert and Sundman.[53] Hallstedt and Gauckler[54] recently reoptimized the Cu-O liquid, obtaining the parameter $^{\circ}G_{Cu^{2+}:Va}$ from the reciprocal relation and giving it a reciprocal energy of 0. This considerably improved the description of the Cu-O liquid and removed the inverted miscibility gap found at high temperatures in the original assessment.[52] An identical strategy is used here. Thus metallic liquid is given by the corner $^{\circ}G^{L}_{Cr^{2+}:Va}$. The parameter $^{\circ}G^{L}_{Cr^{3+}:Va}$ is obtained by the reciprocal reaction given as:

$$^{\circ}G^{L}_{Cr^{3+}:Va} = 2\ ^{\circ}G^{L}_{Cr^{2+}:Va} + {}^{\circ}G^{L}_{Cr^{3+}:O^{2-}} - 3\ ^{\circ}G^{L}_{Cr^{2+}:O^{2-}} + \Delta G_r;$$
$$\Delta G_r = 0 \qquad \text{(Eq 11)}$$

5. Optimization of Parameters

The complete set of optimized thermodynamic parameters describing the Cr-O system is given in Table 2.

The optimization of the thermodynamic parameters was performed using the PARROT module of the Thermo Calc[55] database system. In principle, PARROT can take into account all sorts of thermodynamic and phase diagram data simultaneously. The program minimizes the sum of

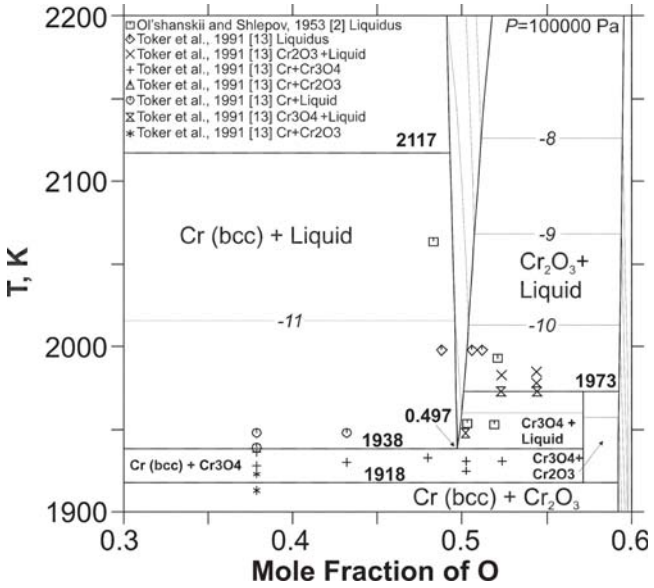

Fig. 4 Enlargement of the calculated Cr-O phase diagram close to the CrO composition, with experimental data and oxygen isobars included

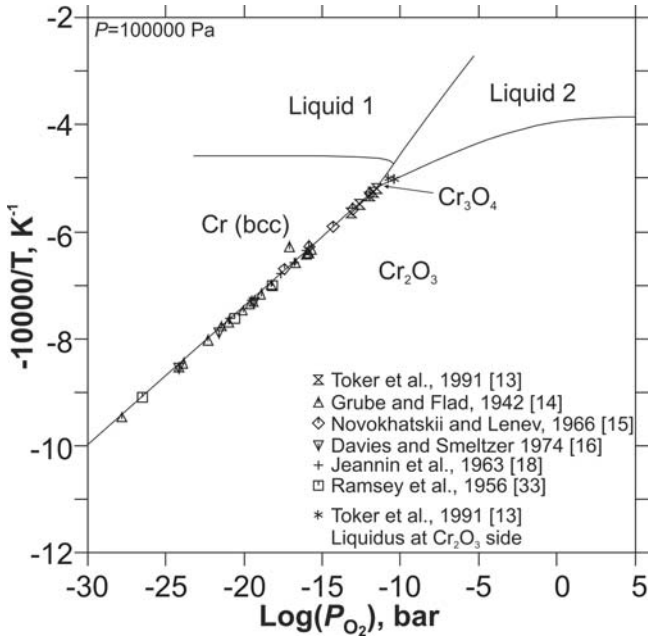

Fig. 5 Calculated oxygen potential phase diagram of the Cr-O system, with experimental log (P_{O_2}) data as a function of temperature from different studies

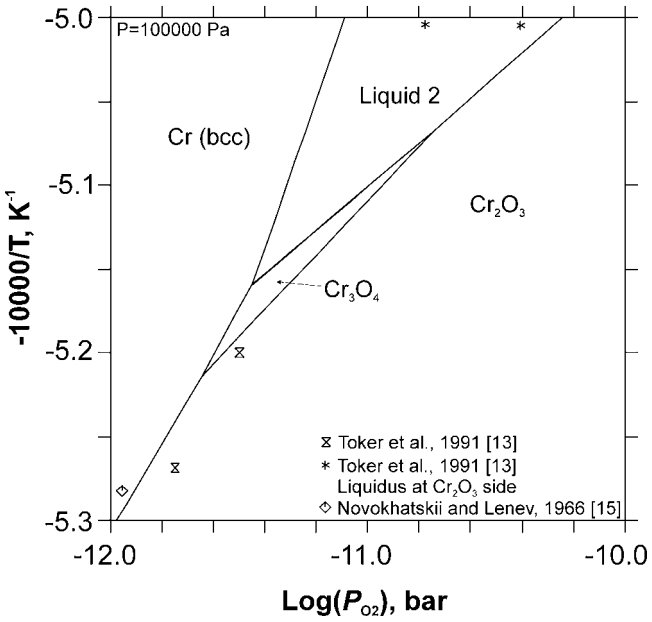

Fig. 6 Stability of Cr_3O_4 in the log (P_{O_2}) versus temperature diagram

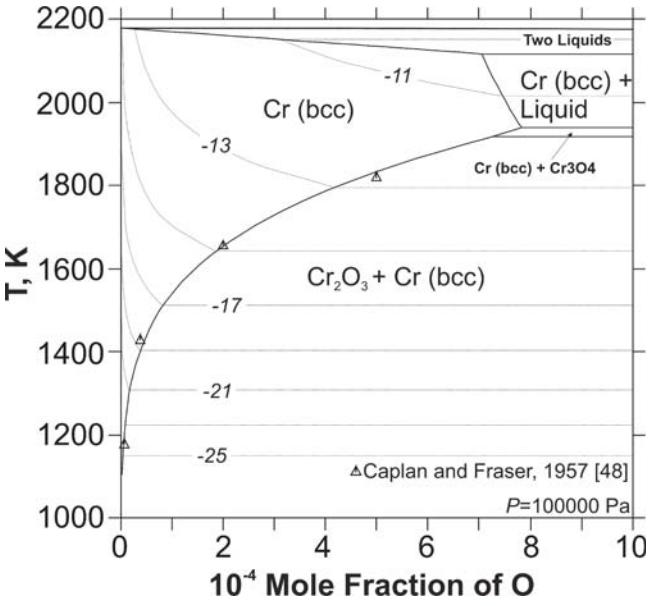

Fig. 7 Calculated oxygen solubility in Cr (bcc) with experimental data and oxygen isobars included

squared errors between the experimentally determined phase diagram and thermodynamic data. As the use of all the experimental data in a simultaneous least square calculation often leads to divergence, the authors selectively adjusted the relative weight of each experimental data point and excluded data that were inconsistent with the majority of the data points during the optimization procedure.

The first parameters to be optimized were the C_p-parameters of Cr_2O_3. These parameters were then kept fixed during the rest of the optimization. The data used were heat content data from Kelley et al.[27] and C_p data from Klemme et al.[25] at 290 K and from 335 to 338 K with a low relative weight. The magnetic parameter for Cr_2O_3, p, is equal to 0.28. The authors optimized T_c and β using C_p data from Klemme et al.[25] close to the antiferromagnetic to paramagnetic transition temperature. To determine the parameters describing the enthalpy and entropy of Cr_2O_3, the authors used log (P_{O_2}) data from Jeannin et al.[18] and Toker et al.,[13] high-temperature emf data from Holzheid and

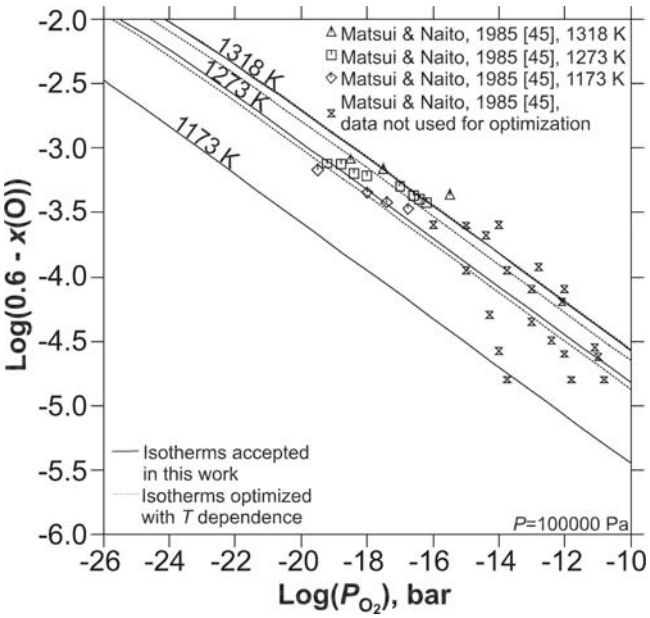

Fig. 8 Optimized nonstoichiometry of $Cr_2O_{3-\delta}$ with the only available experimental data from Matsui and Naito[45] included. Optimization of a temperature dependence is represented by dotted lines. The solid lines result from the authors' accepted optimization without considering temperature dependence. The low nonstoichiometry data show a different slope than the higher nonstoichiometry data.

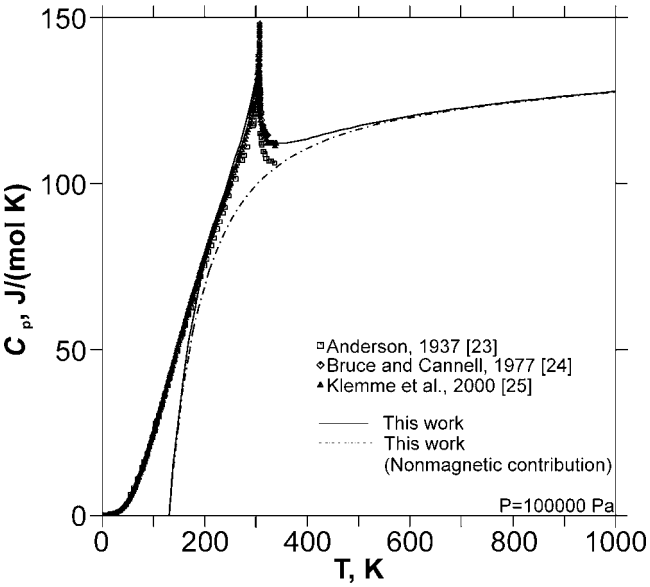

Fig. 9 Comparison of calculated heat capacities of Cr_2O_3 with experimental data

O'Neill,[21] and, with low relative weight, $\Delta_f H^\circ_{298}$ and S°_{298} data from Holzheid and O'Neill.[21] In the next step the authors optimized the nonstoichiometry of $Cr_2O_{3-\delta}$ using data from Matsui and Naito.[45] They assessed Cr_3O_4 and the liquid simultaneously, using experimental phase equilibria data from Toker et al.,[13] experimental data on the liquidus at the oxygen poor side from Toker et al.,[13] and experimental data on the liquidus at the oxygen rich side of the miscibility gap from Ol'shanskii and Shlepov.[2] The melting temperature of eskolaite in air was taken from Bunting.[7] Finally the solubility of O in solid Cr was optimized using data from Caplan et al.[48] In Table 1 values that were used for the authors' optimization are written in italic letters.

6. Results and Discussion

6.1 Phase Diagram

The calculated phase diagram with oxygen isobars is shown in Fig. 3. An enlargement of the phase diagram close to the CrO composition is presented in Fig. 4. The shape of the liquidus on the oxygen poor side of the miscibility gap resulting from the authors' optimization deviates slightly from former optimizations relying on a single experimental datum from Toker et al.[13] and an earlier experiment from Ol'shanskii and Shlepov.[2] The calculated liquidus temperature of eskolaite in air is 2539 K, in good agreement with the measurement from Bunting.[7] For the monotectic temperature of the reaction of Cr (bcc) and liquid, the present authors calculate 2117 K, and for the eutectic one gets 1938 K at a mole fraction of oxygen of 0.497. Cr_3O_4 is formed at 1918 K by a eutectoid reaction $Cr_2O_3 + Cr + \frac{1}{2} O_2 \rightarrow Cr_3O_4$. At a mole fraction of oxygen >0.497 it decomposes in a peritectic reaction at 1973 K that forms Cr_2O_3 and liquid. Figure 5 shows the calculated oxygen potential phase diagram of the Cr-O system with experimental log (P_{O_2}) data included. The experimentally determined phase stabilities from Toker et al.[13] are particularly well reproduced by the authors' optimization. The shape and size of the miscibility gap is speculative due to the lack of experimental data. The stability of Cr_3O_4 is shown in the log (P_{O_2}) versus temperature diagram in Fig. 6. The solubility of oxygen in Cr (bcc) is shown in Fig. 7. For the maximum solubility of oxygen in Cr (bcc) one calculates a mole fraction of oxygen of 0.08 at.% at 1938 K. For the composition of $Cr_2O_{3-\delta}$ one calculates the maximum nonstoichiometry of $Cr_2O_{3-\delta}$ phase with $\delta = 0.098$ to be at 1918 K. The oxygen nonstoichiometry resulting from this optimization might seem somewhat high, but it results simply from the extrapolation of experimental data from Matsui and Naito[45] on oxygen deficiency in function of (P_{O_2}) down to the oxygen partial pressure at the Cr-Cr_2O_3 equilibrium following the proportionality given by the defect chemistry analysis in section 4.1. The comparison of the authors' calculated oxygen nonstoichiometry in $Cr_2O_{3-\delta}$ with the experimental data by Matsui and Naito[45] is given in Fig. 8.The solid lines correspond to the optimization accepted in this work. Obviously the authors' results show a significantly higher temperature dependence compared with the experiments. Considering a temperature dependence for the reduced neutral endpoint of the phase $Cr_2O_{3-\delta}$ gives values of GCRO0 = −202,130 + 235*T* + GCR2O3 + ⅔ GHSERCR (dotted lines in Fig. 8) and leads to the reduced neutral endpoint being too stable at low temperatures. Therefore, due to existing data at only three different

temperatures from a single author, it was decided not to optimize a temperature dependence giving GCRO0 = 108,305 + GCR2O3 + ⅔ GHSERCR. The data at low oxygen nonstoichiometries were not used, as the introduction of an additional defect species would be required to reproduce these.

6.2 Thermodynamic Data

The heat capacities, C_p, of the solid Cr_2O_3 phase (Fig. 9) are well represented by the authors' assessment. For the magnetic parameter β one calculates 3.0, and for T_c one gets 308.6. For $\Delta_f H^\circ_{298}$ (Cr_2O_3) one calculates −1123 kJ/mol, which is in particularly good agreement with the data from Ramsey et al.,[33] and for S°_{298} (Cr_2O_3) one gets 85 J/K · mol, which is very close to the results from Holzheid and O'Neill.[21] For $\Delta_f H^\circ_{298}$ (Cr_3O_4) one calculates −1402 kJ/mol, and for S°_{298} (Cr_3O_4) one gets 175 J/K · mol. These values for Cr_3O_4 deviate significantly from the results of Taylor and Dinsdale,[41] who calculated $\Delta_f H^\circ_{298}$ (Cr_3O_4) = −1447.685 kJ/mol, and S°_{298} (Cr_3O_4) = 150.555 J/K · mol. For a metastable CrO phase one calculates $\Delta_f H^\circ_{298}$ = −306 kJ/mol, and S°_{298} = 46.83 J/K · mol based on the estimates of Shirokov.[30]

7. Conclusions

With the authors' reassessment of the Cr-O system, they are able to describe available thermodynamic and phase diagram data with as few optimizing parameters as possible. However, it must be kept in mind that experimental data on the liquid miscibility gap are largely missing, and that a large variation of the measured melting points of eskolaite exists.

Acknowledgment

This work was financially supported by the Federal Agency for Education and Science, 6th framework program for research and technical development of the European Union, BBW-Nr. 03.170–2.

References

1. S.P.S. Badwal, R. Deller, K. Foger, Y. Ramprakash, and J.P. Zhang, Interaction between Chromia Forming Alloy Interconnects and Air Electrode of Solid Oxide Fuel Cells, *Solid State Ionics,* 1997, **99,** p 297-310
2. Y.I. Ol'shanskii and V.K. Shlepov, Sistema Cr-Cr_2O_3, *Dokl. Akad. Nauk SSSR,* 1953, **91**(3), p 561-564
3. N.Y. Toker, "Equilibrium Phase Relations and Thermodynamics for the Systems Cr-O and Fe-Cr-O in the Temperature Range 1500 to 1825 °C," Thesis, 1978, Pennsylvania State University
4. C.W. Kanolt, Melting Points of Some Refractory Oxides, *J. Wash. Acad. Sci.,* 1913, **3,** p 315-318
5. W.T. Wilde and W.J. Rees, The Ternary System MgO-Al_2O_3-Cr_2O_3, *Brit. Ceram. Trans. J.,* 1943, **42**(7), p 123-155
6. R.N. McNally, F.I. Peters, and P.H. Ribbe, Laboratory Furnace for Studies in Controlled Atmospheres; Melting Points of MgO in a N_2 Atmosphere and of Cr_2O_3 in N_2 and in Air Atmospheres, *J. Am. Ceram. Soc.,* 1961, **44**(10), p 491-493
7. E.N. Bunting, Phase Equilibria in the System Cr_2O_3-Al_2O_3, *J. Res. Nat. Bur. Stand.,* 1931, **6**(6), p 947-949
8. G. Grube and R. Knabe, The System Palladium-Chromium, *Z. Elektrochem.,* 1936, **42**(11), p 793-804, in German
9. R.K.F. Lam, "Melting and Casting of High Purity Chromium with Controlled Oxygen Content," 2000, U.S. Patent 6,039,788
10. D.C. Hilty, W.D. Forgeng, and R.L. Folkman, Oxygen Solubility And Oxide Phases in the Fe-Cr-O System, *T.I. Min. Metall. Eng.,* 1955, **203**(2), p 253-268
11. R.E. Hook and A.M. Adair, The Formation and Dissolution of Chromium Oxides in Chromium, *Trans. Metall. Soc. AIME,* 1964, **230**(6), p 1278-1283
12. R.E. Johnson and A. Muan, Phase Diagrams for the Systems Si-O and Cr-O, *J. Am. Ceram. Soc.,* 1968, **51**(8), p 430-433
13. N.Y. Toker, L.S. Darken, and A. Muan, Equilibrium Phase Relations and Thermodynamics of the Cr-O System in the Temperature Range of 1500 °C to 1825 °C, *Metall. Trans. B,* 1991, **22**(2), p 225-232
14. G. Grube and M. Flad, Affinity and Enthalpy of the Solid Solution in the System Cr-Ni, *Z. Elektrochem.,* 1942, **48**(7), p 377-389, in German
15. A. Novokhatskii and L.M. Lenev, Thermodynamic Properties of Cr_2O_3 and $FeCr_2O_4$ at High Temperatures, *Russ. J. Inorg. Chem.,* 1966, **11**(9), p 1078-1080
16. H. Davies and W.W. Smeltzer, Oxygen and Metal Activities of the Chromium-Nickel-Oxygen System between 900° and 1100 °C, *J. Electrochem. Soc.,* 1974, **121**(4), p 543-549
17. R.D. Pehlke, F.N. Mazandarany, and R.H. Radzilowski, Solid Oxide Electrolyte Emf Cell Determination of the Standard Free Energy of Cr_2O_3 and Applications to Chromium-Bearing Mineral Systems, *Geochim. Cosmochim. Acta,* 1975, **39,** p 833-845
18. Y. Jeannin, C. Mannerskantz, and F.D. Richardson, Activities in Iron-Chromium Alloys, *Trans. Metall. Soc. AIME,* 1963, **227**(2), p 300-305
19. L.A. Pugliese and G.R. Fitterer, Activities and Phase Boundaries in the Cr-Ni System Using a Solid Electrolyte Technique, *Metall. Trans.,* 1970, **1**(7), p 1997-2002
20. J.D. Tretjakow and H. Schmalzried, The Thermodynamics of Spinel Phases (Chromite, Ferrite, Aluminate), *Berich. Bunsen Gesell.,* 1965, **69**(5), p 396-402, in German
21. A. Holzheid and H.S. O'Neill, The Cr-Cr_2O_3 Oxygen Buffer and the Free Energy of Formation of Cr_2O_3 from High-Temperature Electrochemical Measurements, *Geochim. Cosmochim. Acta,* 1995, **59**(3), p 475-479
22. K.T. Jacob, Potentiometric Determination of the Gibbs Free Energy of Formation of Cadmium and Magnesium Chromites, *J. Electrochem. Soc.,* 1977, **124,** p 1827-1831
23. C.T. Anderson, The Heat Capacities of Chromium, Chromic Oxide, Chromous Chloride and Chromic Chloride at Low Temperatures, *J. Am. Ceram. Soc.,* 1937, **59,** p 488-491
24. R.H. Bruce and D.S. Cannell, Specific Heat of Cr_2O_3 Near the Neel Temperature, *Phys. Rev. B,* 1977, **15**(9), p 4451-4459
25. S. Klemme, H.S. O'Neill, W. Schnelle, and E. Gmelin, The Heat Capacity of $MgCr_2O_4$, $FeCr_2O_4$, and Cr_2O_3 at Low Temperatures and Derived Thermodynamic Properties, *Am. Mineral.,* 2000, **85,** p 1686-1693
26. M.W. Chase, C.A. Davies, J.R. Downey Jr., D.J. Flurip, R.A. McDonald, and A.N. Syverud, JANAF Thermochemical Tables, 3rd ed, *J. Phys. Chem. Ref. Data,* 1985, **14**(Suppl. 1), p 940-942
27. K.K. Kelley, F.S. Boericke, E.H. Huffman, and W.M.

Bangert, "Thermodynamic Properties of Carbides of Chromium," Bur. Mines Tech. Paper, No. 662, 1944, 43 pages
28. I. Dellien, F.M. Hall, and L.G. Hepler, Chromium, Molybdenum, and Tungsten: Thermodynamic Properties, Chemical Equilibria, and Standard Potentials, *Chem. Rev.,* 1976, **76**(3), p 283-310
29. D.D. Wagman, W.H. Evans, V.B. Parker, I. Halow, S.M. Bailey, and R.H. Schumm, Selected Values of Chemical Thermodynamic Properties. Tables for Elements 35 through 53 in the Standard Order of Arrangement, *NBS Tech. Note,* 1969, 270(4)
30. N.I. Shirokov, Thermodynamic Properties of Chromous Oxide, *Dokl. Akad. Nauk*, *SSSR, Metal.,* 1973, **2,** p 102-103
31. W.A. Roth and U. Wolf, The Heat of Formation of Chromium Oxide, *Z. Elektrochem.,* 1940, **46,** p 45-46, in German
32. D. Mah, Heats of Formation of Chromium Oxide and Cadmium Oxide from Combustion Calorimetry, *J. Am. Chem. Soc.,* 1954, **76**(13), p 3363-3365
33. J.N. Ramsey, D. Caplan, and A.A. Burr, Thermodynamics of the Oxidation of Chromium, *J. Electrochem. Soc.,* 1956, **103**(2), p 135-138
34. J.P. Coughlin, "Contributions to the Data on Theoretical Metallurgy," Bur. Mines Bull., No. 542, 1954, 80 pages
35. A. Navrotsky, Thermochemistry of Chromium Compounds, Especially Oxides at High Temperature, *Geochim. Cosmochim. Acta,* 1975, **39,** p 819-832
36. R.M. Garrels and C.L. Christ, *Solutions, Minerals and Equilibria,* Harper & Row, 1965, p 410
37. G. Banik, T. Schmitt, P. Ettmayer, and B. Lux, Thermodynamic Consideration on the System Cr-Cr_2O_3, *Z. Metallkd.,* 1980, **71**(10), p 644-645
38. E. Fromm and E. Gebhardt, *Gases and Carbon in Metals,* Springer Verlag, Berlin, Heidelberg, New York, 1976, p 521-534, in German
39. S. Degterov and A.D. Pelton, Critical Evaluation and Optimization of the Thermodynamic Properties and Phase Diagrams of the CrO-Cr_2O_3, CrO-Cr_2O_3-Al_2O_3, and CrO-Cr_2O_3-CaO Systems, *J. Phase Equilib.,* 1996, **17**(6), p 476-487
40. M. Kowalski and P.J. Spencer, Thermodynamic Reevaluation of the Cr-O, Fe-O and Ni-O Systems: Remodelling of the Liquid, BCC and FCC Phases, *Calphad,* 1995, **19**(3), p 229-243
41. J.R. Taylor and A.T. Dinsdale, A Thermodynamic Assessment of the Ni-O, Cr-O and Cr-Ni-O Systems Using the Ionic Liquid and Compound Energy Models, *Z. Metallkd.,* 1990, **81**(5), p 354-366
42. J. Chipman, Atomic Interactions in Molten Alloy Steels, *J. Iron Steel Inst.,* 1955, **180,** p 97-106
43. G. Inden, Determination of Chemical and Magnetic Interchange Energies in BCC Alloys. I. General Treatment, *Z. Metallkd.,* 1975, **66**(10), p 577-582
44. M. Hillert and M. Jarl, A Model of Alloying Effects in Ferromagnetic Metals, *Calphad,* 1978, **2**(3), p 227-238
45. T. Matsui and K. Naito, Existence of Hypostoichiometric Chromium Sesquioxide at Low Oxygen Partial Pressures, *J. Nucl. Mater.,* 1985, **136,** p 78-82
46. E.W.A. Young, J.H. Gerretson, and J.H.W. de Witt, The Oxygen Partial-Pressure Dependence of the Defect Structure of Chromium(III)Oxide, *Elec. Chem. Soc.,* 1987, **134**(9), p 2257-2260
47. A.N. Grundy, E. Povoden, T. Ivas, and L.J. Gauckler, Calculation of Defect Chemistry Using the CALPHAD Approach, *Calphad,* 2005, **30,** p 33-41
48. D. Caplan, M.J. Fraser, and A.A. Burr, in *Ductile Chromium,* American Society for Metals, Cleveland, OH, 1957, p 196
49. A.T. Dinsdale, SGTE Data for Pure Elements, *Calphad,* 1991, **15**(4), p 344-346
50. M. Hillert, B. Jansson, B. Sundman, and J. Ågren, A Two-Sublattice Model of Molten Solutions with Different Tendency of Ionization, *Metall. Trans. A,* 1985, **16A,** p 261-266
51. B. Sundman, Modification of the Two-Sublattice Model for Liquids, *Calphad,* 1991, **15,** p 109-119
52. B. Hallstedt, D. Risold, and L.J. Gauckler, Thermodynamic Assessment of the Copper-Oxygen System, *J. Phase Equilib.,* 1994, **15**(5), p 483-499
53. M. Hillert and B. Sundman, Predicting Miscibility Gaps in Reciprocal Liquids, *Calphad,* 2001, **25**(4), p 599-605
54. B. Hallstedt and L.J. Gauckler, Revision of the Thermodynamic Descriptions of the Cu-O, Ag-O, Ag-Cu-O, Bi-Sr-O, Bi-Cu-O, Sr-Cu-O, Ca-Cu-O and Sr-Ca-Cu-O Systems, *Calphad,* 2003, **27**(2), p 177-191
55. B. Sundman, B. Jansson, and J.O. Andersson, The Thermo-Calc Databank System, *Calphad,* 1985, **9**(2), p 153-190